Review

Directly Synthesized Graphene-Based Photonics and Optoelectronics Devices

Siam Uddin [1,2] and Yong-Won Song [1,2,*]

[1] Center for Opto-Electronic Materials and Devices, Korea Institute of Science and Technology, Seoul 02792, Korea; siam_uddin@kist.re.kr
[2] Division of Nano and Information Technology, University of Science and Technology, Daejeon 34113, Korea
[*] Correspondence: ysong@kist.re.kr

Abstract: In the past two decades, extensive research and studies have been performed on graphene because of its exceptional physical properties. Owing to its ultrahigh carrier mobility, quantum Hall effect and unique optical transmittance, graphene is considered to be a multi-functional component for realizing next-generation optoelectronic and photonic devices. Significant efforts have been made towards efficient synthesis, transfer, and integration of graphene for use in device scale. However, the critical hurdles lie in developing 3D and conformal graphene, which are ideal for integrated hybrid photonic systems. Here, we review different methods of synthesizing graphene, specifically recent advances in the synthesis of direct, conformal, 3D graphene. In addition, we comprehensively summarize the latest progress made towards directly grown, 3D, conformal graphene-based photonic and optoelectronic applications. Finally, several important challenges for large-sale implementation of directly grown graphene-based optoelectronic and photonic devices are discussed.

Keywords: direct synthesis of graphene; 3D graphene; ACS method; optical nonlinearity; graphene photonics; ultrafast laser; ultrafast optical switching

1. Introduction

In the recent past, silicon technology has dominated the electronic-to-data communication system of modern society. However, the industry is currently striving to meet the demand of faster and more efficient data processing, as the potential of silicon-based components seems to have reached a limit [1,2]. Accordingly, there have been recent discoveries in 2D materials and related studies to match the requirements of modern times. Hence, in the intense competition for the next dominant technology, graphene is considered to be a competent candidate.

Graphene is an exquisite 2D material comprising a one-atom-thick planar sheet of sp^2-bonded carbon atoms. The structural configuration of graphene is a hexagonal honeycomb crystal that contains six carbon atoms. These atoms form strong σ-bonds and additional π–π* bonds by hybridization of the p^z orbitals of the immediate carbon atoms in the hexagon. Graphene acts like a metal with a vanishing Fermi surface or a semiconductor having zero bandgap. This is due to its conduction and valance bands being symmetrical at the Dirac point where π–π and π*–π* overlap and result in a Fermi surface pin. The π electrons of graphene are compelled to have a low-energy band structure that resemble two symmetric cones representing valence and conduction bands that contact at the Dirac point at energies lower than 1 eV. Electron diffusion in this energy zone is known to be linear to a larger extent, akin to that of light, and unlike other conventional 2D materials with parabolic dispersion. The low-energy electronic arrangement is a spinor characteristic of graphene that regulates the inhibition of backscattering, which is a dominating factor for graphene with excellent transfer properties [3–7]. Nevertheless, graphene is an ideal photonic and optoelectronic material due to the broadband optical properties [8–14]. The aforementioned

characteristics forge the path for graphene to be a potential material for optoelectronic and photonic applications [15–30].

Graphene synthesis was first accomplished by applying techniques such as micro- mechanical rift and epitaxial growth on SiC at elevated temperatures. For practical utilization, it is imperative to use synthesis methods that produce defect free, high quality graphene. Therefore, only limited approaches, such as mechanical exfoliation, carbon nanotube unzipping, epitaxial growth, self-assembly of surfactants, chemical vapor deposition (CVD), and chemical conversion, have been employed by researchers to synthesize graphene to meet the conditions of practical utilization [31–38]. Synthesis of monolayer graphene on a larger scale was achieved by large improvements to the CVD technique [39–45]. However, these approaches cannot ensure direct use of graphene in devices for many notable reasons, such as the use of metal catalysts, chemical etching of catalytic materials, transfer or exfoliation, complex chemical reactions, and high operational temperatures.

More importantly, it has been seen that optoelectronic and photonic devices are usually compact and not always planar; therefore, the transfer of 2D graphene synthesized by the prevailing methods onto practical non-planar, curvilinear, or customized substrates has critical limitations and disadvantages. Additionally, graphene is usually damaged under the mechanical and chemical stress of post-transfer treatment [46–49]. Therefore, a transfer-free, direct synthesis of graphene on arbitrary surfaces is highly anticipated for the development of optoelectronic and photonic devices. Furthermore, in the case of optoelectronic and photonic devices, it is not possible to exploit the efficient light-graphene interaction because 2D graphene cannot cover 3D devices in a conformal manner. Accordingly, an advanced study of graphene synthesis that promises to be more direct, less complex, cost-efficient, and readily applicable to 3D structures for device manufacturing is highly demanded, confirming the utilization of the potentials that graphene offers.

In this review, we present a brief summary of growth of graphene on metal catalysts and dielectric substrates through CVD. Additionally, transfer-free and direct synthesis of graphene realized in most recently adopted processes, in situ growth, and atomic carbon spraying (ACS) are discussed in this review. The demonstration of the excellent optical properties of the resultant graphene derived from the direct synthesis methods for use in optical devices is also discussed.

2. Growth Mechanism of Graphene

2.1. Conventional Methods of Graphene Synthesis

Since the discovery of graphene, extensive research has been conducted regarding the synthesis of graphene. Amongst all the conventional methods of graphene production, CVD on catalytic metal substrates seems to be one of the better prospective strategies. There are several available reports on the synthesis of graphene with Ni and Cu catalysts [40,42,43,50,51], as well as various other metal catalysts, such as Co [52], Ru [53], Ir [54], Pt [55], Re [56], and Pd [57] that have been employed for CVD-based synthesis of graphene.

In the case of the Ni-catalyst-based synthesis, polycrystalline Ni films are annealed at 900–1000 °C under an Ar/H$_2$ atmosphere to increase the grain boundaries, facilitating the growth of graphene with larger grain size [43,58]. The Ni films were then exposed to hydrocarbons to initiate the growth process. The hydrocarbon gas is decomposed into C atoms, which dissolve in bulk Ni. Because Ni possesses high carbon solubility [59], the dissolved C atoms continue to form Ni–C solid bonds until the C atoms reach a super saturation state in the Ni film. Consequently, monolayer graphene forms by C segregation, which can be observed on the surface [60]. The outcome of CVD-based synthesis of graphene using Ni catalysts is highly dependent on the temperature used. The higher the temperature, the more the carbon solubility Ni possesses. When the temperature is cooled down, more C atoms start diffusing from the solid Ni-C solution and start precipitating out to the Ni surface, thereby forming a graphene film of a certain thickness [61–63]. In addition to temperature, the microstructure of Ni plays a vital role in graphene formation [43,50,51].

The grain boundaries in polycrystalline Ni substrates lead to the formation of multilayer graphene, whereas the Ni (111) substrate renders a smooth surface, which results in graphene uniformity.

In an experiment to produce graphene [43], the synthesis was performed over Ni films. The Ni films were deposited on a SiO_2/Si substrate by e-beam evaporation, as shown in the optical image in Figure 1a and then was annealed at an elevated temperature before the synthesis process in CVD. After exposure of the polycrystalline Ni film to highly diluted CH_4 flow under ambient pressure at $900-1000$ °C, an atomically thin (1–10 layers) graphene film was grown on the Ni surface. Formation of single- and multi-layered films bridge together yielding a continuous film of graphene crystal. Figure 1b presents the optical image of the transferred resultant graphene, demonstrating the preservation of the geometry of the transferred film. Furthermore, the grain size at micrometer scale from the transferred graphene film calculated by Raman spectroscopy (as presented in Figure 1c) shows the advantages of annealing the Ni film in the synthesis process.
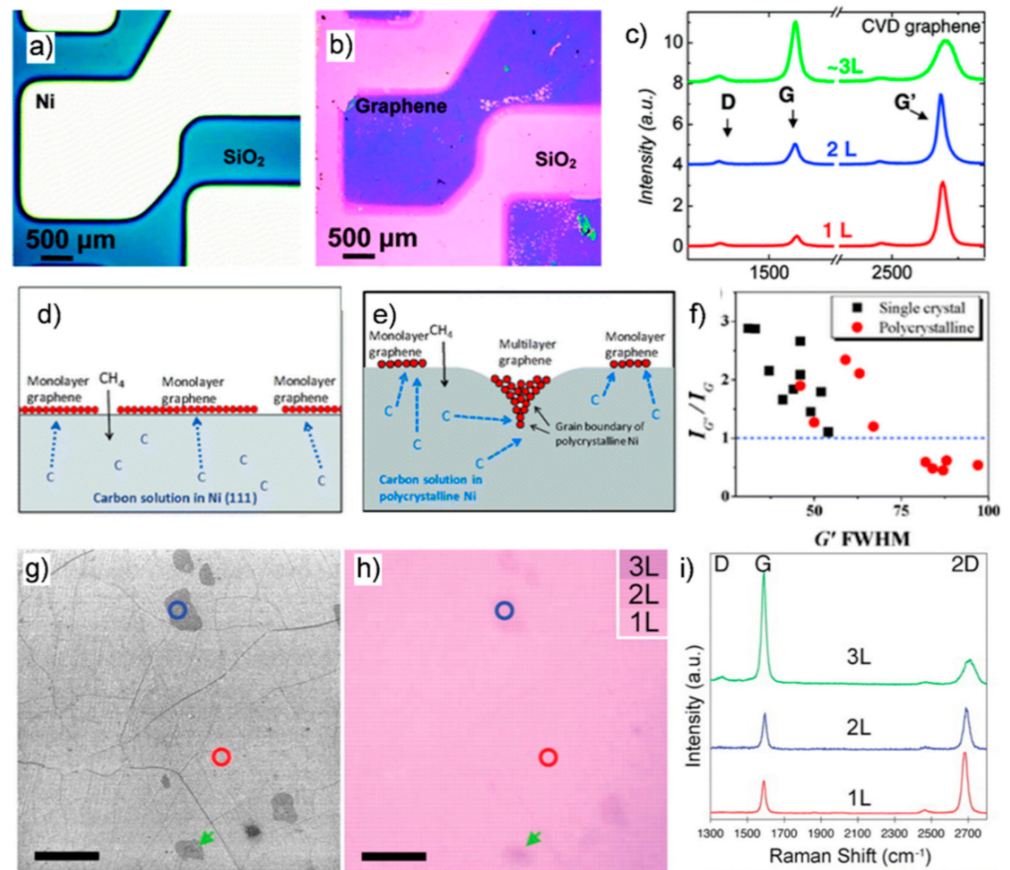

Figure 1. Metal catalyst assisted growth of graphene: (**a**) Micrograph of a patterned Ni film on SiO_2/Si; (**b**) Micrograph of the grown graphene transferred to targeted SiO_2/Si substrate; (**c**) Raman spectroscopy of the transferred graphene film; (**d**) Schematic presentation of graphene growth mechanism on Ni (111); (**e**) Schematic diagrams of graphene growth mechanism on polycrystalline Ni surface; (**f**) The $I_{G'}/I_G$ intensity ratio versus the FWHM of G' peak of graphene grown on Ni (111) and polycrystalline Ni; (**g**) SEM image of the transferred graphene; (**h**) Micrograph of the transferred graphene; (**i**) Raman spectra taken from different points of the transferred graphene film. (**a**–**c**) Reproduced with permission from [43]. Copyright American Chemical Society, 2009; (**d**–**f**) Reproduced with permission from [58]. Copyright American Chemical Society, 2010; (**g**–**i**) Reproduced with permission from [42]. Copyright Science, 2009.

Another study reported that [58] multilayer graphene domain formation is influenced by the concentration of Ni boundaries based on the precipitation of carbon atoms [64]. Single-crystalline Ni (111) film favors the growth of mono/bilayer graphene with higher uniformity, which hinders the growth of multilayer graphene. In contrast, polycrystalline Ni facilitates the growth of multilayer graphene. The researchers synthesized graphene on both single-crystalline (in Figure 1d) and polycrystalline Ni (in Figure 1e) surfaces. The growth temperature was elevated up to 900 °C under H_2 ambience.

After the CVD growth process, micro-Raman spectroscopy verified the uniform formation of graphene layers on both of the Ni surfaces; formation of monolayer/bilayer graphene accounted for 91.4% of the area for single-crystalline Ni contrasting to 72.8% for that of polycrystalline Ni (as portrayed in Figure 1f) under comparable growth condition. The Raman peaks of Ni (111) and polycrystalline Ni are assigned to the G and G' (D band was negligible) bands of the graphene layers, respectively, confirming that the graphene produced on both surfaces have low defects [58].

The CVD process on polycrystalline Cu foils was performed by Rouff et al. in a similar setup like that used for Ni [42]. However, unlike Ni, Cu has no partially filled d-orbital that can interact with C atoms; therefore, Cu possesses ultralow carbon solubility. Furthermore, the graphene formation on Cu is not a case of segregation and precipitation but a surface reaction process. This means that the graphene growth process is controlled by surface-absorption growth in the case of Cu, where the carbon decomposes from the hydrocarbon on the Cu surface. From the beginning of nucleation, the formation of graphene domains continues progressively until the decomposition of the precursor hydrocarbon becomes super-saturated. Therefore, the growth mechanism is a self-limiting process, generally resulting in high surface coverage by a monolayer. This mechanism has been verified with isotope variant precursor molecule-based growth and Raman characterization [65].

Because graphene and Cu have different thermal expansion coefficients, graphene "wrinkles" can be seen in Figure 1g (SEM image) and Figure 1h (optical image). The "wrinkles" can also go across Cu grain boundaries, indicating that multilayer graphene is not formed in the grain boundaries and the transferred graphene film is continuous. Further speculation with Raman spectra can be made based on Figure 1i, in which the peaks assigned as D, G, and 2D bands carry information, such as defect density and film thickness. In addition, the D map proves the uniformity of the as-grown graphene, except for the regions where wrinkles are visible that are close to the multilayer regions. The G and 2D maps clearly show the existence of multilayer graphene in the flakes. By analyzing all the SEM characterizations, the amount of monolayer graphene was found to be 95%, less than 1% of monolayer/trilayer graphene and 3–4% of bilayer graphene [42].

2.2. Interfacial Growth

A considerable number of issues, such as wrinkles, cracks, contamination, low efficiency in the growth process, and complex transferring procedures, are undeniable in metal-catalyst-based conventional CVD-grown graphene [66,67]. Therefore, transfer-free graphene synthesis methods attracted significant attention among researchers. Interfacial growth process enables the growth of a patterned graphene layer between the substrate and catalyst layers; it is a method conceived to avoid the transferring process by optimizing critical growth factors that affect the synthesis mechanism [68–70].

A study confirmed that synthesis of graphene can be obtained at the interface of the substrate and Ni film inside a generic CVD furnace [71]. Figure 2a–d provide a pictorial presentation of the synthesis procedure. There was no external carbon source fed to the furnace, and no transfer process was required after the synthesis.

In this process, an electron beam (e-beam) evaporator was used for Ni deposition, where the substrates were heated at 1000 °C and then cooled to room temperature to sustain nucleation and growth of the graphene crystals. Large grain boundaries were obtained after applying high-temperature heat treatment, which can be controlled by optimizing the thermal conditions. According to the study, no external carbon sources were required

as high carbon density near the grain boundary (GB) and the high-speed diffusion paths for the carbon atoms were confirmed by the duplicated weak patterns of Ni-GB on the graphene layer [72].

The Raman spectrum of the as-grown graphene presented in Figure 2e illustrates that a few layers of graphene were grown at the interface that corresponded well with the TEM analysis. In another study [73], high carbon density and diffused carbon atoms were obtained from the Ni grain boundaries in the resultant graphene, which advances the process without any external carbon source [71,73]. The prepared graphene was studied by Raman spectroscopy; the graphene grown at 710 °C was found to be more crystalline than that grown at 700 °C.

Another study revealed a diffusion-assisted synthesis (DAS) method, in which graphene was synthesized on SiO_2/Si substrate, plastics, or glass [74]. A Ni film was employed as a catalyst, and solid carbon was used as a carbon source to form a graphene layer under an electron evaporator within a wide range of working temperatures (from 25 °C on PMMA and glass to 400 °C on SiO_2/Si (100)). In this work, thermally oxidized Si (100), poly(methyl methacrylate) (PMMA)-covered SiO_2, and commercially available glass were used as substrates. For the catalyst material, a thin Ni film (~100 nm) was deposited on the substrates, and then annealed at 1000 °C in an H_2 atmosphere to yield a strong 111-texture and micrometer-sized grains with smooth surfaces. Ni is used for possessing high carbon solubility, and Ni (111) is nearly lattice-matched with the basal planes of graphite; these two important factors provide equal epitaxial growth of graphene [64,75]. The source was solid C, which was supplied from a paste made of graphite powder dispersed in ethanol. The molybdenum holding stage was used for applying a homogeneous pressure (<1 MPa) to the C-Ni/substrate. This ensured efficient contact at the C–Ni interface and stimulated the C–C bond breaking on the catalytic Ni (111) surface [76,77]. Subsequently, the sample was sealed in a quartz tube, which was filled with inert argon gas and heated for a short time between 25 and 260 °C. The C-Ni film was treated using an $FeCl_3$ solution to obtain the resultant graphene layer. From the Raman spectra, it was confirmed that a few layers of synthesized graphene were found on SiO_2 and the as-synthesized graphene films were wrinkle-free and smooth over large areas. The average grain size was found to be approximately 5–20 μm for the Ni/SiO_2 arrangement and 40–50 nm for the Ni on plastic and glass substrates. Furthermore, the estimated carrier (hole) mobility of the graphene-enabled field-effect transistor was found to be 667 cm^2 V^{-1} s^{-1} at room temperature.

Transfer-free growth of multilayer graphene using the self-assembled monolayers (SAM) method was reported in [78], which is efficient and promising because the amount of carbon can be easily controlled [79–81]. In this process, SiO_2/Si, quartz, GaN, and textured Si were used as substrates. First, the targeted substrates were cleaned thoroughly with acetone/isopropyl alcohol and piranha solutions (1:3 mixture of hydrogen peroxide and sulfuric acid). Later, the substrates were immersed in 0.1 M trimethoxyphenylsilane (PhSi(OMe)$_3$, Sigma-Aldrich solution in hexane overnight followed by thermal annealing at 120 °C for 20 min to prepare the phenyl-SAM/substrate structure. Then an electron-beam evaporator was used on top of the SAM for Cu (200 nm) or Ni films (300 nm) deposition. To form a Cu/graphene/substrate structure, a low-vacuum furnace was loaded with the prepared samples at 600−1000 °C. Subsequently, 1 wt. % ammonium persulfate was used to wet-etch the Cu films. High-quality graphene was produced on SiO_2/Si and quartz substrates, although further optimization of growth conditions is required for GaN and textured Si. The transfer-free growth method for graphene proposed in this study uncovers new possibilities for industrial graphene-based device applications. Raman spectroscopy further shows the effect of flow rates of Ar and H_2 on the quality of the synthesized graphene, as shown in Figure 2f. Raman analysis revealed that a high flow rate of Ar is required for the optimal growth of graphene under certain conditions.
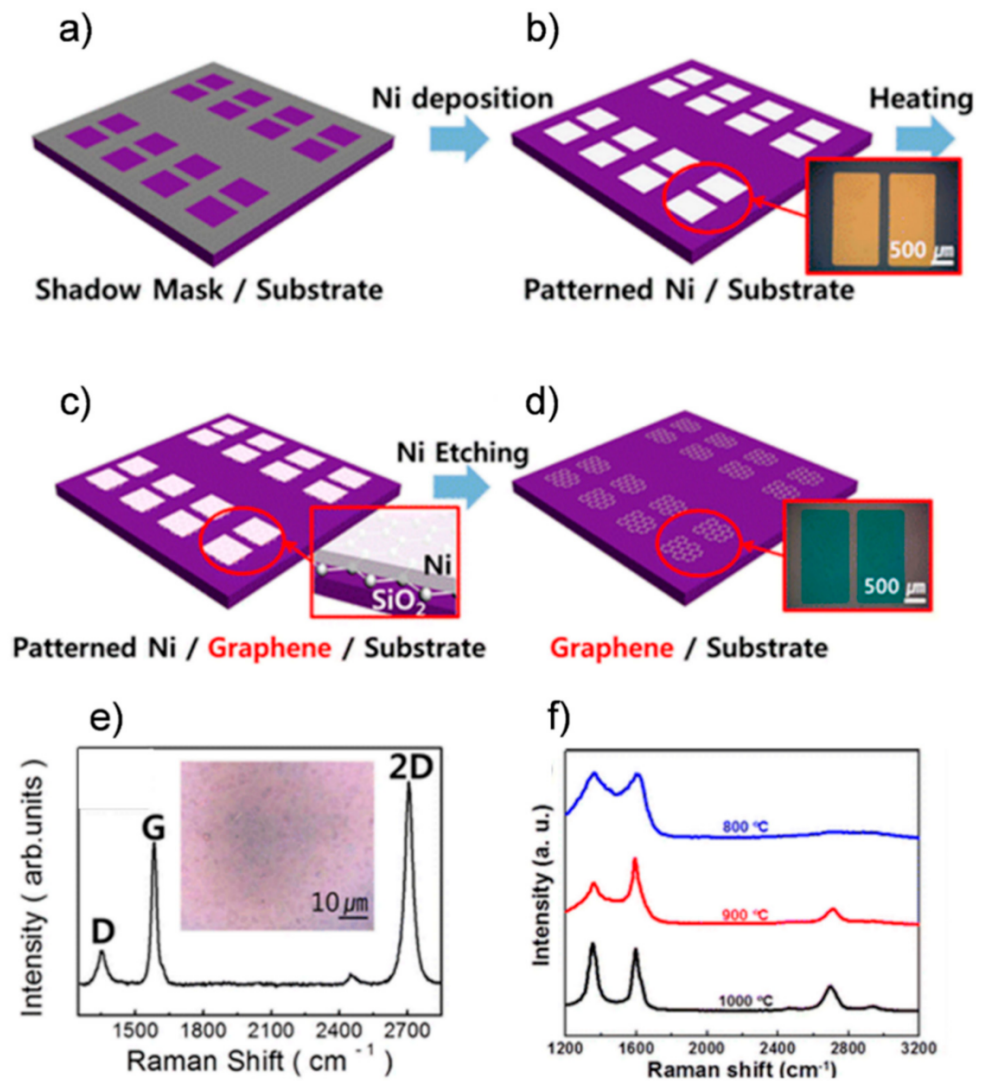
Figure 2. (**a**–**d**) Graphical representation of the experimental procedure of interfacial growth of graphene without any source feeding; (**e**) Raman spectrum of as-grown graphene on SiO_2/Si substrate from (**a**–**d**); (**f**) Temperature functional growth of graphene on SiO_2/Si substrate and evolution of Raman spectra. (**a**–**e**) Reproduced with permission from [71]. Copyright American Chemical Society, 2012; (**f**) Reproduced with permission from [78]. Copyright American Chemical Society, 2016.

2.3. In-Situ Growth

To synthesize graphene on an optical device under ambient conditions, a transfer-free, in-situ growth process has been proposed that can grow graphene directly onto single-mode optical fiber end facets [82] and on the flat surface of a side-polished single-mode fiber (SMF) under ambient atmospheric conditions [83] as schematicized in Figure 3a,b, respectively. In this method, on the end facet and polished region, a polycrystaline Ni film was pre-deposited, which acted as a catalyst for interfacial growth as well as a host for the C atoms. The authors first deposited a 100 nm thin film of polycrystalline Ni on the ferrule end facet and on the flat surface of a side-polished SMF using the electron beam evaporation method. Two CW lasers at 1552 (pump) and 1539 (probe) nm were coupled such that the incident pump and probe laser could be reflected back from the Ni layer or interacted with the Ni layer and monitored accordingly. During light irradiation, the optical power of the pump laser was tuned from 0 to 7 dBm by a 0.5 dB step every 30 min, while the power of the probe laser was fixed at −1.26 dBm. With the absorption of the light-induced heat, carbon atoms will segregate and precipitate on the grain boundaries of the Ni film [66–70,84–86].

After light irradiation, a 0.2 M iron (III) chloride ($FeCl_3$) solution was used to etch out the Ni layer by placing the laser-exposed parts in the solution for 30 min. This process yielded the SMF parts grown with interfacial graphene. The graphene-incorporated device was employed for ultrafast pulse generation and optical switching in furtherance.
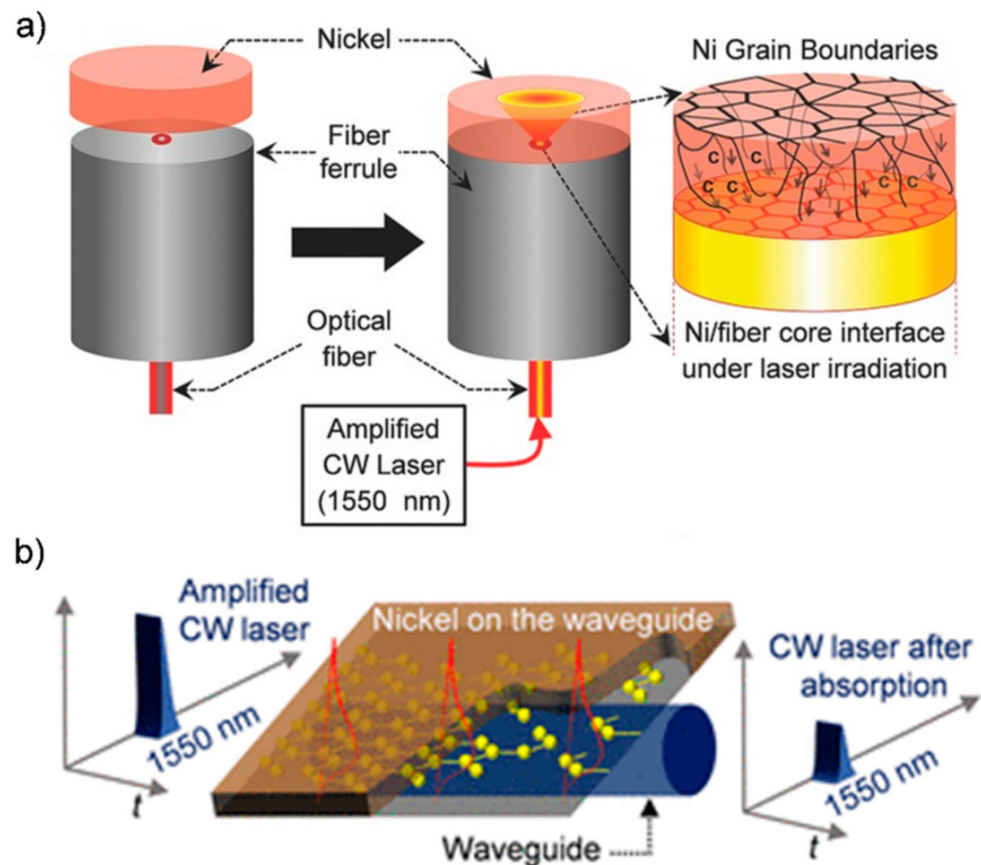

Figure 3. (**a**) Schematic representation of the laser induced synthesis of graphene by the in-situ method onto SMF end facet; (**b**) Schematic illustrations of in-situ synthesis of graphene onto the flat surface of a D-shaped fiber. (**a**) Reproduced with permission from [82]. Copyright WILEY-VCH Verlag GmbH & Co. KGaA, Weinheim, 2015. (**b**) Reproduced with permission from [83]. Copyright American Chemical Society, 2018.

2.4. Metal-Free Growth Technique

Direct growth techniques on metal oxide substrates are encouraging, as these substrates avoid deleterious transfers and exhibit an insulating nature. Catalytic graphene growth has been analyzed on sapphire [87,88], quartz [89,90], and SiO_2 [90], but these are considered to be high-temperature reactions. Although using MgO [91,92] or ZrO_2 [92] substrates reduced the processing temperature (~350 °C), high surface diffusion barrier of C atoms, small band gaps, uneven growth of graphene [91,92], and high leakage current density (~1×10^{-4} A cm^{-2}) [93,94] are considered to be limitations.

The fabrication of a ready-to-use graphene sticker comprising a polymer spin-coat and separated by peeling off the polymer film [95] are shown schematically in Figure 4a,b. Then, graphene/γ-Al_2O_3 is scaled off from the additional layers. Atomic layer deposition (ALD) is used to deposit the initial amorphous Al_2O_3, which later transforms into gamma phase at elevated temperatures. The transformed γ-Al_2O_3 acted as a substrate inside the CVD furnace where dehydrogenation of CH_4 occurred.

Another study [96] introduced the generation of nanographene (nGr) on γ-Al_2O_3, where a weak adhesion was observed between the graphene and substrate; therefore,

the synthesized nGr film was easily separable, and no conventional chemical [60,97,98] etchant was required. The sheet resistance (R_s) was found to be increased in the grown nGr [90,99,100], which is an indication of a reduction in the grain population.
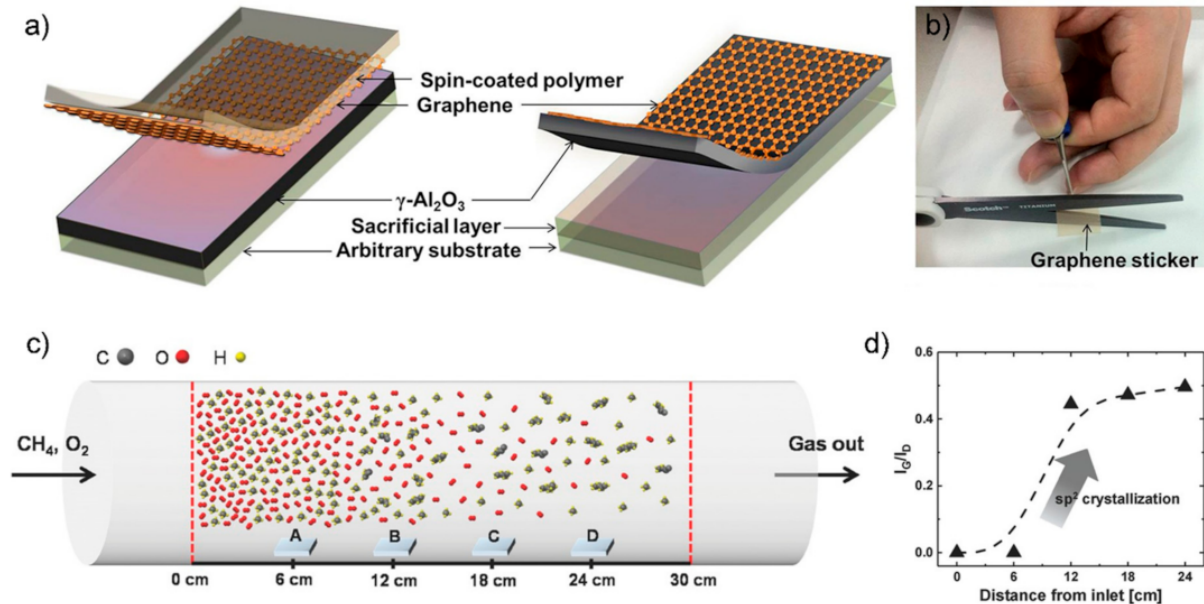

Figure 4. (**a**) Graphical representations of preparing readily detachable graphene sticker; (**b**) Photograph of processing of graphene sticker; (**c**) Molecular dynamics during adsorption process on Al(III) sites; (**d**) Distance dependent Raman intensity ratio indicating change in sp^2 formation; (**a**,**b**) Reproduced with permission from [95]. Copyright Scientific Reports, 2015. (**c**,**d**) Reproduced with permission from [101]. Copyright WILEY-VCH Verlag GmbH & Co. KGaA, Weinheim, 2017.

The outcome of oxygen being present during graphene synthesis on a ceramic catalyst has been inspected in a study [101], which observed the effect of graphene grown at distinct oxygen exposures with altering positions inside the CVD furnace. This inspection confirmed that the O_2 influx from the system leakage acted as a growth inhibitor for graphene. Oxygen leakage in CVD systems has adverse effects, as it leads to defects in the grown graphene [99,102]. The presence of oxygen modifies the contact resistance and sheet resistance; these were found to directly influence the device performance [103–105]. In this experiment, the highly reactive tri-coordinated $Al_{(III)}$ sites on γ-Al_2O_3 surfaces acted as catalytic sites because they possess strong reactivity [101,106,107]. Leaked oxygen reacted on these $Al_{(III)}$ sites, as schematized in Figure 4c.

By increasing the distance between the inlet and substrate, the oxygen and sp^3 portions declined from 25.76% to 10.59% and from 21.15% to 14.70%, respectively. Meanwhile, the values of I_G/I_D, which is the ratio of the G-peak intensity (corresponding to the graphene crystal) to the D-peak intensity (corresponding to the defect), have been found to be inversely functional to the distance from the inlet, as shown in Figure 4d. By examining the sample grown at different positions, different values of sheet resistance (R_s) were found. Within the 0–6 cm position from the inlet, the value of R_s approached infinity, whereas the samples at the 12, 18, and 24 cm positions had R_s values of 6.64, 1.06, and 0.64 kΩ sq^{-1}, respectively.

2.5. Conformal Graphene Growth on Silicon Nanostructures

A recent report [108] describes the conformal growth of graphene on SiNH structure that worked as a photo-detecting device. In their process, silver-assisted etching method along with discretely distributed silver nanoparticles (AgNPs) was employed to form the SiNH structures as shown in Figure 5a. Low-pressure radio frequency (RF) PECVD technique was used to grow conformal graphene on the SiNH structures. Finally,

photolithography, vacuum evaporation, and dry etching were performed to fabricate the conformal graphene/SiNH-based photodetectors. After characterization by TEM, layers of graphene of 10 and 5–7 folds were found on the apexes and the sidewalls of the SiNH nanocones, respectively. In addition, as seen from Figure 5b, the Raman spectra also show the growth of graphene with some defects on the SiNHs morphologies.
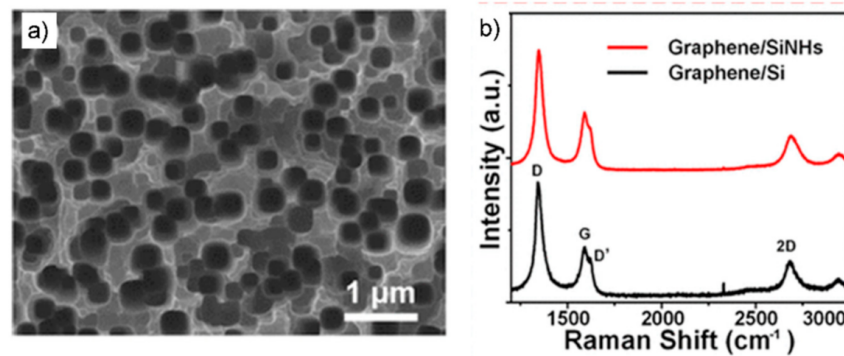

Figure 5. (**a**) SEM image of the conformal graphene/SiNHs structure; (**b**) Raman spectra of graphene on SiNHs (red) and Si (black); (**a**,**b**) Reproduced with permission from [108]. Copyright American Chemical Society, 2019.

2.6. Synthesis of Graphene by the ACS Method

Despite striving persistently to grow 3D graphene, which is in demand for practical electronic, optoelectronic, and optical devices, the inadequacy of synthetic methods and the practice of conventional transfer approaches have limited its realization. Accordingly, a metal-free, etching-free, transfer-free, direct synthesis method of functional graphene that contours 3D-structured surfaces of nonlinear optical devices has been proposed in [109]. In this method, first, the catalytic effect of γ-Al$_2$O$_3$, i.e., the ceramic material employed as the growth catalyst, was verified by synthesizing graphene on it. Inside the CVD furnace, dehydrogenation of CH$_4$ occurs on the surface of γ-Al$_2$O$_3$, resulting in the generation of C atoms at lower activation energies. As the density of C atoms increases, the concentration gradient of C atoms between the catalyst and the target surfaces evolves gradually. The increasing concentration gradient leads to the development of a driving force for C atoms to flow through air towards the neighboring surface via surface diffusion and undergo graphitization. Accordingly, the graphene clusters on the neighboring surface resemble the "sprayed" C atoms from the catalyst. This mechanism has been defined as the ACS method and is graphically presented in Figure 6a.
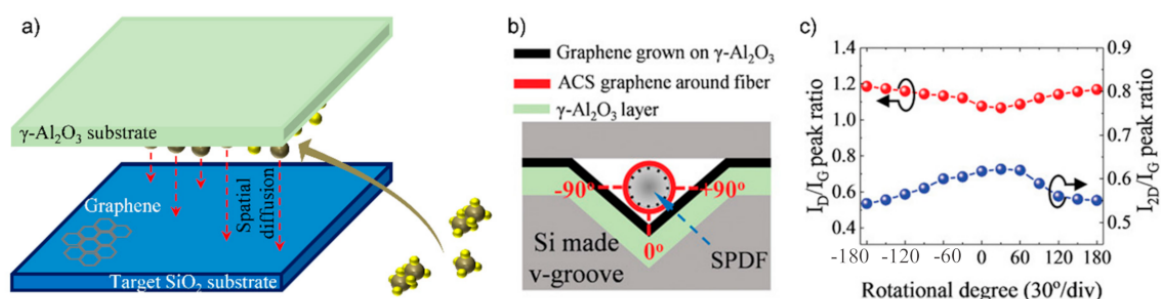

Figure 6. (**a**) Schematic representation of graphene growth on the targeted surface by spatial diffusion; (**b**) Schematic of the setup for synthesizing graphene around the 3D structured fiber by the ACS process; (**c**) Raman intensity ratio of I$_D$/I$_G$ (red curve) and I$_{2D}$/I$_G$ (blue curve) acquired from the fiber perimeter. (**a**–**c**) Reproduced with permission from [109]. Copyright WILEY-VCH Verlag GmbH & Co. KGaA, Weinheim, 2020.

To fabricate a practical 3D structured optical device coated with conformal 3D graphene by the ACS method, a V-shaped groove pre-deposited with a γ-Al_2O_3 thin film and covered with a SiO_2 substrate from the top was employed, as shown in Figure 6b. The grown graphene around the fiber was further analyzed by evaluating both I_D/I_G and I_{2D}/I_G peak ratios, as presented in Figure 6c. The region nearest to the fiber from the γ-Al_2O_3 surface during synthesis (from $-90°$ to $+90°$ in Figure 6b) was coated with higher-quality graphene compared to other regions, which indicates the impact of a longer distance between γ-Al_2O_3 and the number of O_2 atoms on the growth of graphene. This method requires no metal catalyst, has less complexity, and yet produces high quality graphene growth. Owing to the ability to control semiconducting properties by tuning the growth condition, this process has a higher potential for further functional systems than the conventional techniques.

3. Application of Directly Grown Graphene

3.1. Ultrafast Fiber Laser

The excellent optical properties of graphene, such as its broadband saturable absorption, ultra-wide spectral range because of the straight scattering of Dirac electrons, unique energy band gap, and ultrafast recovery time, makes it suitable for ultrafast pulse generation and a powerful element for fiber lasers [110]. Several studies have proven that graphene can be an excellent SA for both mode-locking and Q-switching pulse generation in infrared wavelengths [111–121]. However, directly synthesized graphene contouring the surfaces of the 3D-structured optical devices is highly anticipated to maximize the nonlinear interaction with guided light. Here, we have discussed two processes, in situ and ACS, that enable growing graphene directly on the optical devices so that no further transferring is required. Accordingly, by providing maximum surface coverage and eliminating the interstices that frequently have been found for the suspended graphene cases, maximum light-matter interaction can be ensured [109].

A SA device, made of in situ grown graphene on the fiber end facet, as shown in Figure 7a, was employed to generate soliton pulses. The central wavelength and full width at half maximum (FWHM) of the generated ultrafast pulses were found to be λ = 1571.96 nm and 0.75 nm, respectively, as shown in Figure 7b. The pulse repetition rate was determined to be *frep* = 15.06 MHz with a pulse duration of 2.6 ns for sech^2-profile as shown in Figure 7c. Later, as presented in Figure 7d, the in situ grown graphene on the polished surface of a D-shaped fiber device was employed in the same cavity to achieve femtosecond pulses. In this case, the generated pulse was centered at 1559 nm with a FWHM of 3.44 nm (see Figure 7e), where the pulse repetition rate was determined to be 8.93 MHz (see inset of Figure 7e); the generated pulse was found in the fs scale with a measured duration of 910 fs (see Figure 7f). The time-bandwidth product (TBP) value of 0.386, indicating the output pulses were slightly chirped, was calculated from the pulses. These results indicate the stability of the soliton pulses generated by in situ graphene.

Thereafter, another work reveals generating ultrafast pulses by a metal-free, transfer-free, directly synthesized conformal graphene synthesized by the ACS method [109]. mboxfigfig:applsci-1118015-f007g schematically illustrates how the ACS-grown graphene can maximize the nonlinear interaction, compared to the case of graphene transferred by conventional methods. In this study, the central wavelength of the pulses from an ACS grown graphene-enabled SA device reported to be λ = 1555.82 nm with an FWHM of 3.75 nm. The solitonic operation was found until 16.15 mW of intracavity power, beyond which the pulses were found to be stretched (see Figure 7h). The pulse duration in the temporal domain and TBP was 770 fs (see Figure 7i) and 0.35, respectively.
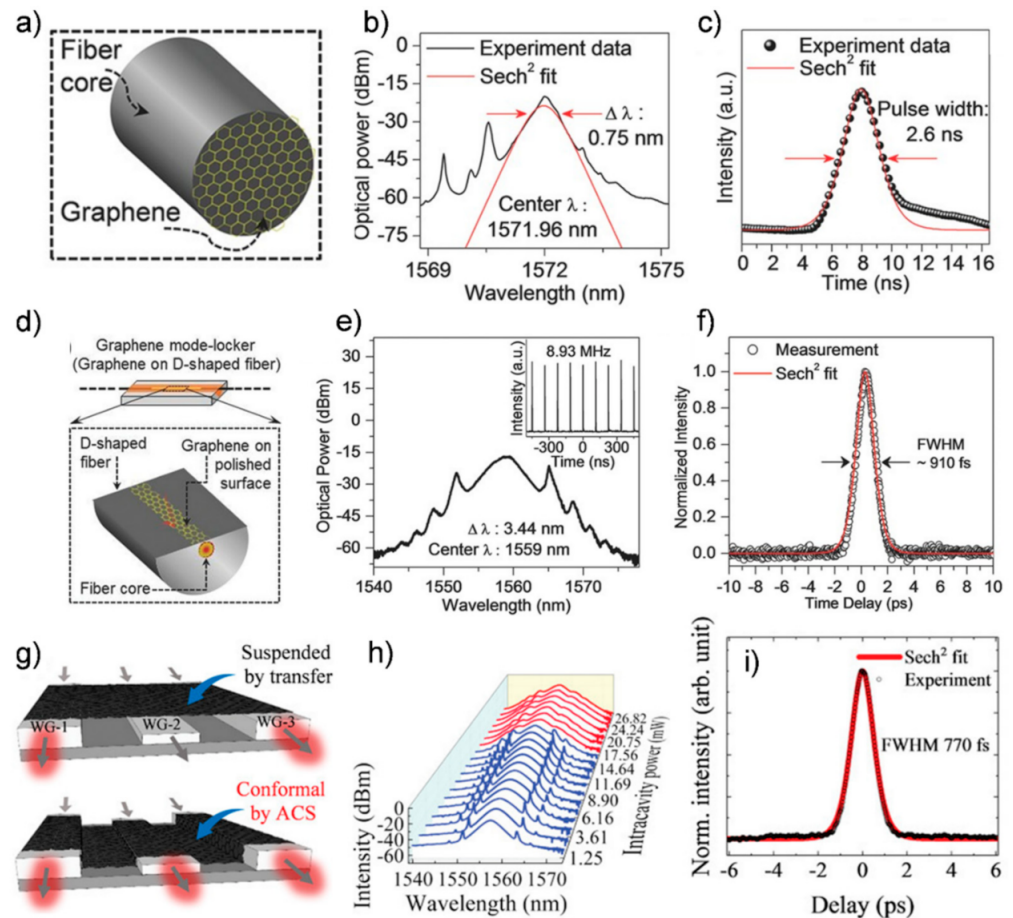
Figure 7. (**a**) Schematics of the mode-locker device made from in-situ grown graphene on SMF end facet; (**b**) Output characteristics of pulse spectrum in wavelength domain mode-locked with device shown in (**a**); (**c**) Pulse duration with the mode-locker device shown in (**a**); (**d**) Schematics of mode-locker device made from in-situ grown graphene on the flat face of a D-shaped fiber; (**e**) Output characteristics of pulse spectrum in wavelength domain mode-locked with device shown in (**d**); (**f** Pulse duration with mode-locker device shown in (**d**); (**g**) Superiority of ACS-grown graphene over transferred graphene; (**h**) Intracavity power dependent optical spectra of the pulses; (**d**) Duration of the mode-locked pulses. (**a–f**) Reproduced with permission from [82]. Copyright WILEY-VCH Verlag GmbH & Co. KGaA, Weinheim, 2015. (**g–i**) Reproduced with permission from [109]. Copyright WILEY-VCH Verlag GmbH & Co. KGaA, Weinheim, 2020.

3.2. Ultrafast Optical Switching

In FWM, new frequency components can be generated either by using two strong pumps ($\omega_1 \neq \omega_2$), which is called the non-degenerate case, or one strong pump ($\omega_1 = \omega_2$), which is called the degenerate case.

FWM is a nonlinear optical Kerr effect derivative that occurs if two waves propagate through a nonlinear medium simultaneously and generate one or two new waves. However, by attaching an optically nonlinear material to the polished surface of an optical fiber, the newly produced signal, based on the FWM concept, can be enhanced to enable ultrafast optical switching for ultra-high-speed optical communication systems. It has already been demonstrated by previous studies that various nonlinear 2D materials, such as carbon nanotubes and black phosphorus (BP) are suitable for FWM [122,123]. However, considering all the new features in the electronic and optical realms, such as nonlinear optical switching, FWM with graphene could be a new pathway for the computational design of systems and applications.

To investigate the FWM process with in situ grown graphene, two CW lasers were employed for the demonstration: one for launching the pump channel and another for the modulated signal channel (tunable) at λ_p = 1552.4 nm and λ_s = 1559 nm, respectively [83]. The resulting wavelengths of the newly produced optical channels were λ_{Chg1} = 1545 nm and λ_{Chg2} = 1566 nm for the aforementioned pump channel and signal channel (see Figure 8a), respectively. The in situ graphene-coated D-shaped fiber had a 2 dB (58.5% nonlinear increment) higher value of ER, as indicated in Figure 8b, than that of the bare D-shaped fiber.

To exploit ultrafast optical switching with ACS grown graphene demonstrated the values of pump and signal channel wavelengths of λ_p = 1551.92 nm and λ_s = 1555.46 nm, respectively. Due to the optical nonlinearity derived from ACS grown graphene, the newly generated signal channels were found at 1559.01 nm and 1548.39 nm, respectively, by the ultrafast FWM process. By employing an ACS graphene-coated nonlinear device, 2.23 dB (an increase of 67% of the nonlinear process) nonlinear enhancement at 20 GHz modulation frequency was recorded by calculating the extinction ratio (ER) difference between with and without ACS graphene cases [109]. Figure 8c shows the evolution of the spectral broadening in the produced channels with the separation of the sidebands as the modulation frequency is increased for ACS grown graphene. To evaluate the detuning experiment using an ACS-grown-graphene-enabled optical device, the pump channel was fixed at 1551.92 nm, while the modulated launched signal channel wavelength was tuned up to 11.828 nm with a resolution of 0.2 nm. Additionally, the negligible phase mismatching issue in the FWM experiment was confirmed by analyzing the ER curves of the detuning data with (blue curve) and without (gray curve) the ACS graphene cases, and similar trends were found at the local maxima and minima points, as displayed in Figure 8d.
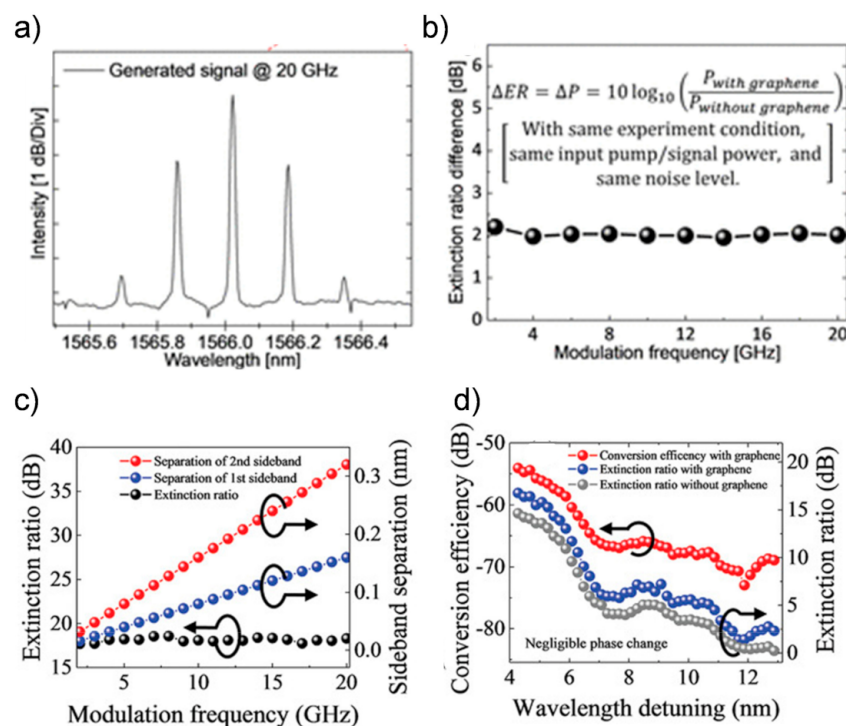

Figure 8. (**a**) Generated signal corresponding to original signal; (**b**) Extinction ratio (ER) comparison for without and with in-situ graphene cases; (**c**) Modulation frequency dependent sideband separation in FWM demonstration with ACS graphene; (**d**) Wavelength detuning dependent conversion efficiency (red curve) and ER (blue curve) for confirming negligible phase-mismatch during FWM experiment. (**a**,**b**) Reproduced with permission from [83]. Copyright American Chemical Society, 2018; (**c**,**d**) Reproduced with permission from [109]. Copyright WILEY-VCH Verlag GmbH & Co. KGaA, Weinheim, 2020.

3.3. Photodetection

A technique of explicit growth of graphene coatings on the surface of silicon nanoholes (SiNHs) through plasma enhanced chemical vapor deposition (PECVD) was projected to accomplish transfer-free conformal graphene/SiNH photo detectors for the first time [108]. The conformal graphene/SiNH structures were found to have an exceptional light absorption pursuance with absorptions risen up to 90%, and also consist high power absorption densities, that results in more photo carrier procreations per unit volume in the SiNHs than planar silicon. It was found that the photocurrent of the conformal graphene/SiNH photo detector is likely to be 34 μA, which is definitely much higher than the other fellows: planar graphene/Si (17 μA) and SiNHs (10 μA) as shown in Figure 9a. Consequently, the photo response speeds of three kinds of photo detectors, as shown in Figure 9b, were evaluated with respect to the light modulation frequencies at 1, 100, and 2500 Hz, and the results for the conformal graphene/SiNH photo detector were found to be satisfactory. For all switching frequencies, the photo detectors can switch swiftly between "on" and "off" states. Hence, the conformal graphene/SiNH photo detectors are quicker than the other two detectors because the carriers originated in SiNHs can infuse into the nearby conformal graphene more promptly. These consequences emerge from the lower reflections, higher absorption densities, and shorter carrier transport paths in conformal graphene/SiNH detectors.
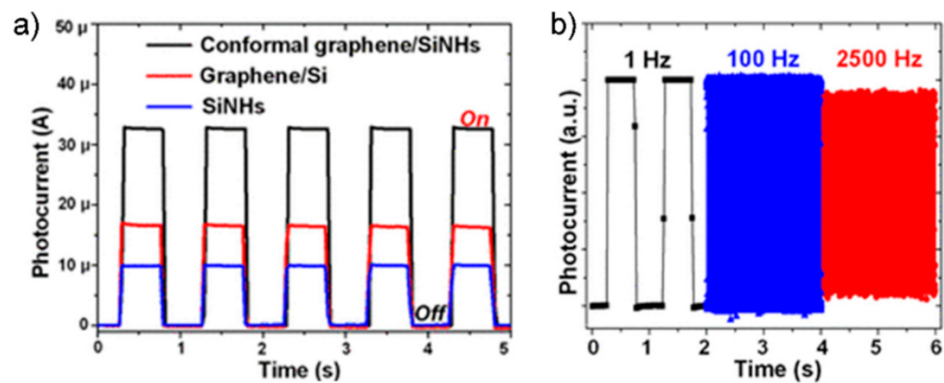

Figure 9. (**a**) Photoresponse of the graphene/Si, SiNHs, and conformal graphene/SiNH photodetectors; (**b**) Photoresponse of the proposed photodetectors at 1, 100, and 2500 Hz of frequencies. (**a**), (**b**) Reproduced with permission from [108]. Copyright American Chemical Society, 2019.

4. Future Perspectives

Despite the long history of graphene and its unique electronic and optical properties, practical demonstration and production methods for synthesizing a promising quality of graphene have not yet been achieved. The conventional methods of graphene synthesis have faced difficulties, resulting in reduced process efficiency. Graphene synthesis, as a result, has not yet reached its full potential. The most important development driving research of direct graphene growth has been in the area of transfer-free growth. Directly grown graphene is a favorable solution, as it could elevate the performance of chip-scale integration for graphene-based optical devices with a minimum footprint. In addition, it can be applied to both ultrafast optical and nanoelectronic device manufacturing, and thus develop prevailing technology in the fields of nanoelectronics, photonics, optical communications, and optical computing.

The critical challenge for realizing optoelectronic and photonic devices with directly synthesized graphene is its quality. The current methods for direct growth of graphene are not sufficiently precise to apply industrially, as the quality of the resultant graphene is inferior to that of the quality of conventionally synthesized graphene. Thus, a breakthrough to develop high-quality graphene from direct growth mechanisms, as well as further related studies, is required. Furthermore, the controllability of the nano-graphene nucleation dynamics during synthesis is an engaging area of development.

Another major issue is the growth temperature for graphene synthesis; the available reports on directly synthesized graphene discuss high temperature growth, while low temperature growth results are poor in quality and insufficient for implementation on a device scale. Further, application-based investigations on the synthesis of directly grown graphene are scarce. The progress towards growing graphene directly in the required quality and size at low temperatures on a non-catalytic substrate is therefore painstaking. It might be possible to reduce the production cost of graphene by reducing the growth temperature; however, crystallinity, uniformity, quality, and size of the resultant graphene are the major points to be considered. Therefore, developing new schemes to achieve the ultimate goal of a direct, defect-free graphene-based optical device should be the primary focus point. Efficient light-graphene interaction is another crucial factor in the production of ultrafast photonic devices, which cannot be achieved from 2D graphene structures. Moreover, to minimize scattering loss during the light-graphene interaction, a high-quality thin film of graphene is desired.

5. Conclusions

We present a brief review of recent advancements in the development of directly synthesized graphene-based optoelectronic and photonic devices. In addition to the exciting electronic and optical properties, we have first discussed the current state of the art for synthesis of graphene. Then, we presented a summary of directly synthesized graphene on optical fiber-based substrates that exploit its nonlinear optical responses. Combined with facile direct growth and no requirements for transferring the resultant graphene, these methods are promising for applications in electronics and nonlinear optical ultrafast photonic devices. In addition to the superior coverage of graphene by the direct method, conformal growth is a great benefit that nullifies interstices frequently observed in suspended graphene cases. Nevertheless, the distance (distance from catalyst to the target substrates) functional growth of graphene exhibits tunable semiconducting properties that can be exploited for nanoelectronic devices. Demonstrations of ultrafast optical pulses in both Q-switching and mode-locking domains with in-situ and ACS grown graphene-enabled devices were possible. Ultrafast optical switching up to 20 GHz modulation frequency has been demonstrated by graphene grown in situ, and ACS methods indicate that the optical nonlinearity is sufficiently high. In addition to their excellent electronic and optical properties, these direct growth methods strengthen the candidacy of graphene for optoelectronic and photonic devices. The verified optical nonlinearity with direct growth methods on fiber devices can pave the way for implementation in futuristic graphene-enabled hybrid optoelectronic and photonic devices.

The in situ and ACS methods, evidently different from other conventional methods, can develop transfer-free, directly synthesized graphene on optical devices. Furthermore, the ACS method has exhibited potential as a practical solution for direct synthesis of graphene on arbitrary 3D substrates. This method is a breakthrough for future on-chip optical signal processing and optical interconnects along with the chip-scale integration of electro-optic hybrid devices. In recent studies, the possibility of graphene-based integrated devices has been analyzed. Thus, graphene can also be used in broad-ranging optical control schemes. Therefore, the fabrication of silicon-based integrated optical circuits, which are expected to be used in numerous operations, such as pulsed light generation, routing, modulation, computing, and detection, can be enabled. Moreover, the integration of graphene into hybrid silicon photonics could be possible by direct deposition of graphene onto silicon. Therefore, graphene research may spawn a technological revolution that could possibly turn into a paradigm shift for ultrafast optics.

References

1. Waldrop, M.M. The chips are down for Moore's law. *Nat. Cell Biol.* **2016**, *530*, 144–147. [CrossRef]
2. Schulz, M. The end of the road for silicon? *Nat. Cell Biol.* **1999**, *399*, 729–730. [CrossRef]
3. Neto, A.C.; Guinea, F.; Peres, N.M.; Novoselov, K.S.; Geim, A.K. The electronic properties of graphene. *Rev. Mod. Phys.* **2009**, *81*, 109. [CrossRef]
4. Allen, M.J.; Tung, V.C.; Kaner, R.B. Honeycomb Carbon: A Review of Graphene. *Chem. Rev.* **2010**, *110*, 132–145. [CrossRef] [PubMed]
5. Avouris, P. Graphene: Electronic and Photonic Properties and Devices. *Nano Lett.* **2010**, *10*, 4285–4294. [CrossRef]
6. Geim, A.K.; Novoselov, K.S. The rise of graphene. *Nat. Mater.* **2007**, *6*, 183–191. [CrossRef] [PubMed]
7. Das Sarma, S.; Adam, S.; Hwang, E.H.; Rossi, E. Electronic transport in two-dimensional graphene. *Rev. Mod. Phys.* **2011**, *83*, 407–470. [CrossRef]
8. Nair, R.R.; Blake, P.; Grigorenko, A.N.; Novoselov, K.S.; Booth, T.J.; Stauber, T.; Peres, N.M.R.; Geim, A.K. Fine Structure Constant Defines Visual Transparency of Graphene. *Science* **2008**, *320*, 1308. [CrossRef] [PubMed]
9. Hasan, T.; Sun, Z.; Wang, F.; Bonaccorso, F.; Tan, P.H.; Rozhin, A.G.; Ferrari, A.C. Nanotube–polymer composites for ultrafast photonics. *Adv. Mater.* **2009**, *21*, 3874–3899. [CrossRef]
10. Yamashita, S. A Tutorial on Nonlinear Photonic Applications of Carbon Nanotube and Graphene. *J. Light. Technol.* **2011**, *30*, 427–447. [CrossRef]
11. Lui, C.H.; Mak, K.F.; Shan, J.; Heinz, T.F. Ultrafast Photoluminescence from Graphene. *Phys. Rev. Lett.* **2010**, *105*, 127404. [CrossRef] [PubMed]
12. Wu, Y.; Wang, B.; Ma, Y.; Huang, Y.; Li, N.; Zhang, F.; Chen, Y. Efficient and large-scale synthesis of few-layered graphene using an arc-discharge method and conductivity studies of the resulting films. *Nano Res.* **2010**, *3*, 661–669. [CrossRef]
13. Hendry, E.; Hale, P.J.; Moger, J.J.; Savchenko, A.K.; Mikhailov, S.A. Coherent Nonlinear Optical Response of Graphene. *Phys. Rev. Lett.* **2010**, *105*, 097401. [CrossRef]
14. Zhang, H.; Virally, S.; Bao, Q.; Ping, L.K.; Massar, S.; Godbout, N.; Kockaert, P. Z-scan measurement of the nonlinear refractive index of graphene. *Opt. Lett.* **2012**, *37*, 1856–1858. [CrossRef]
15. Han, M.Y.; Oezyilmaz, B.; Zhang, Y.; Kim, P. Energy Band-Gap Engineering of Graphene Nanoribbons. *Phys. Rev. Lett.* **2007**, *98*, 206805. [CrossRef] [PubMed]
16. Lemme, M.C.; Echtermeyer, T.J.; Baus, M.; Kurz, H. A Graphene Field-Effect Device. *IEEE Electron Device Lett.* **2007**, *28*, 282–284. [CrossRef]
17. Lin, Y.-M.; Dimitrakopoulos, C.; Jenkins, K.A.; Farmer, D.B.; Chiu, H.-Y.; Grill, A.; Avouris, P. 100-GHz transistors from wafer-scale epitaxial graphene. *Science* **2010**, *327*, 662. [CrossRef] [PubMed]
18. Lee, S.; Kim, J.T.; Song, Y.-W. Graphene-Incorporated Soft Capacitors for Mechanically Adjustable Electro-Optic Modulators. *ACS Appl. Mater. Interfaces* **2018**, *10*, 40781–40788. [CrossRef] [PubMed]
19. Lee, S.; Song, Y.-W. Graphene Self-Phase-Lockers Formed around a Cu Wire Hub for Ring Resonators Incorporated into 57.8 Gigahertz Fiber Pulsed Lasers. *ACS Nano* **2020**, *14*, 15944–15952. [CrossRef]
20. Ryu, B.; Kim, J.T.; Song, Y.-W. Graphene-dispersed polymer waveguide for efficient formation of mode-locked lasers at extremely low graphene concentration. *Carbon* **2020**, *166*, 123–130. [CrossRef]
21. Ryu, B.; Lee, S.; Kim, J.T.; Song, Y.-W. Efficient Optical Saturable Absorbers with Graphene on Polymer Waveguides for Femtosecond Laser Pulse Formation. *Ann. Phys.* **2018**, *530*. [CrossRef]
22. Kovalchuk, O.; Uddin, S.; Lee, S.; Song, Y.-W. Graphene Capacitor-Based Electrical Switching of Mode-Locking in All-Fiberized Femtosecond Lasers. *ACS Appl. Mater. Interfaces* **2020**, *12*, 54005–54011. [CrossRef]
23. Bao, Q.; Zhang, H.; Yang, J.-X.; Wang, S.; Tang, D.Y.; Jose, R.; Ramakrishna, S.; Lim, C.T.; Loh, K.P. Graphene-Polymer Nanofiber Membrane for Ultrafast Photonics. *Adv. Funct. Mater.* **2010**, *20*, 782–791. [CrossRef]

24. Zheng, Z.; Zhao, C.; Lu, S.; Chen, Y.; Li, Y.; Zhang, H.; Wen, S. Microwave and optical saturable absorption in graphene. *Opt. Express* **2012**, *20*, 23201–23214. [CrossRef] [PubMed]

25. Liu, M.; Yin, X.; Ulin-Avila, E.; Geng, B.; Zentgraf, T.; Ju, L.; Wang, F.; Zhang, X. A graphene-based broadband optical modulator. *Nat. Cell Biol.* **2011**, *474*, 64–67. [CrossRef] [PubMed]

26. Gao, Y.; Shiue, R.-J.; Gan, X.; Li, L.; Peng, C.; Meric, I.; Wang, L.; Szep, A.; Walker, D.; Hone, J.; et al. High-Speed Electro-Optic Modulator Integrated with Graphene-Boron Nitride Heterostructure and Photonic Crystal Nanocavity. *Nano Lett.* **2015**, *15*, 2001–2005. [CrossRef]

27. Tong, S.W.; Wang, Y.; Zheng, Y.; Ng, M.-F.; Loh, K.P. Graphene Intermediate Layer in Tandem Organic Photovoltaic Cells. *Adv. Funct. Mater.* **2011**, *21*, 4430–4435. [CrossRef]

28. Wu, J.; Agrawal, M.; Becerril, H.A.; Bao, Z.; Liu, Z.; Chen, Y.; Peumans, P. Organic Light-Emitting Diodes on Solution-Processed Graphene Transparent Electrodes. *ACS Nano* **2009**, *4*, 43–48. [CrossRef]

29. Xia, F.; Mueller, T.; Golizadeh-Mojarad, R.; Freitag, M.; Lin, Y.-M.; Tsang, J.; Perebeinos, V.; Avouris, P. Photocurrent Imaging and Efficient Photon Detection in a Graphene Transistor. *Nano Lett.* **2009**, *9*, 1039–1044. [CrossRef]

30. Mueller, T.; Xia, F.; Avouris, P. Graphene photodetectors for high-speed optical communications. *Nat. Photon* **2010**, *4*, 297–301. [CrossRef]

31. Kim, W.S.; Moon, S.Y.; Park, N.-H.; Huh, H.; Shim, K.B.; Ham, H. Electrical and Structural Feature of Monolayer Graphene Produced by Pulse Current Unzipping and Microwave Exfoliation of Carbon Nanotubes. *Chem. Mater.* **2011**, *23*, 940–944. [CrossRef]

32. Li, N.; Wang, Z.; Zhao, K.; Shi, Z.; Gu, Z.; Xu, S. Large scale synthesis of N-doped multi-layered graphene sheets by simple arc-discharge method. *Carbon* **2010**, *48*, 255–259. [CrossRef]

33. Pang, S.; Englert, J.M.; Tsao, H.N.; Hernandez, Y.; Hirsch, A.; Feng, X.; Müllen, K. Extrinsic Corrugation-Assisted Mechanical Exfoliation of Monolayer Graphene. *Adv. Mater.* **2010**, *22*, 5374–5377. [CrossRef] [PubMed]

34. Poon, S.W.; Chen, W.; Tok, E.S.; Wee, A.T.S. Probing epitaxial growth of graphene on silicon carbide by metal decoration. *Appl. Phys. Lett.* **2008**, *92*, 104102. [CrossRef]

35. Shen, B.; Ding, J.; Yan, X.; Feng, W.; Li, J.; Xue, Q. Influence of different buffer gases on synthesis of few-layered graphene by arc discharge method. *Appl. Surf. Sci.* **2012**, *258*, 4523–4531. [CrossRef]

36. Sinitskii, A.; Fursina, A.A.; Kosynkin, D.V.; Higginbotham, A.L.; Natelson, D.; Tour, J.M. Electronic transport in monolayer graphene nanoribbons produced by chemical unzipping of carbon nanotubes. *Appl. Phys. Lett.* **2009**, *95*, 253108. [CrossRef]

37. Suk, J.W.; Lee, W.H.; Kang, T.J.; Piner, R.D.; Won, S.J.; Hyoung, L.W.; June, K.T. Transfer of Chemical Vapor Deposition-Grown Monolayer Graphene by Alkane Hydrocarbon. *Sci. Adv. Mater.* **2016**, *8*, 144–147. [CrossRef]

38. Tan, H.; Fan, Y.; Rong, Y.; Porter, B.; Lau, C.S.; Zhou, Y.; He, Z.; Wang, S.; Bhaskaran, H.; Warner, J.H. Doping Graphene Transistors Using Vertical Stacked Monolayer WS2 Heterostructures Grown by Chemical Vapor Deposition. *ACS Appl. Mater. Interfaces* **2016**, *8*, 1644–1652. [CrossRef]

39. Bae, S.; Kim, H.K.; Lee, Y.; Xu, X.; Park, J.-S.; Zheng, Y.; Balakrishnan, J.; Lei, T.; Kim, H.R.; Song, Y.I.; et al. Roll-to-roll production of 30-inch graphene films for transparent electrodes. *Nat. Nanotechnol.* **2010**, *5*, 574–578. [CrossRef]

40. Kim, K.S.; Zhao, Y.; Jang, H.; Lee, S.Y.; Kim, J.M.; Kim, K.S.; Ahn, J.-H.; Kim, P.; Choi, J.-Y.; Hong, B.H. Large-scale pattern growth of graphene films for stretchable transparent electrodes. *Nature* **2009**, *457*, 706–710. [CrossRef]

41. Lee, S.; Lee, K.; Zhong, Z. Wafer Scale Homogeneous Bilayer Graphene Films by Chemical Vapor Deposition. *Nano Lett.* **2010**, *10*, 4702–4707. [CrossRef] [PubMed]

42. Li, X.; Cai, W.; An, J.; Kim, S.; Nah, J.; Yang, D.; Piner, R.; Velamakanni, A.; Jung, I.; Tutuc, E.; et al. Large-Area Synthesis of High-Quality and Uniform Graphene Films on Copper Foils. *Science* **2009**, *324*, 1312–1314. [CrossRef]

43. Reina, A.; Jia, X.; Ho, J.; Nezich, D.; Son, H.; Bulovic, V.; Dresselhaus, M.S.; Kong, J. Large Area, Few-Layer Graphene Films on Arbitrary Substrates by Chemical Vapor Deposition. *Nano Lett.* **2009**, *9*, 30–35. [CrossRef]

44. Sun, Z.; Yan, Z.; Yao, J.; Beitler, E.; Zhu, Y.; Tour, J.M. Growth of graphene from solid carbon sources. *Nat. Cell Biol.* **2010**, *468*, 549–552. [CrossRef]

45. Yan, K.; Peng, H.; Zhou, Y.; Li, H.; Liu, Z. Formation of Bilayer Bernal Graphene: Layer-by-Layer Epitaxy via Chemical Vapor Deposition. *Nano Lett.* **2011**, *11*, 1106–1110. [CrossRef]

46. Su, C.-Y.; Lu, A.-Y.; Xu, Y.; Chen, F.-R.; Khlobystov, A.N.; Li, L.-J. High-Quality Thin Graphene Films from Fast Electrochemical Exfoliation. *ACS Nano* **2011**, *5*, 2332–2339. [CrossRef] [PubMed]

47. Ishigami, M.; Chen, J.H.; Cullen, W.G.; Fuhrer, M.S.; Williams, E.D. Atomic Structure of Graphene on SiO₂. *Nano Lett.* **2007**, *7*, 1643–1648. [CrossRef]

48. Pirkle, A.; Chan, J.; Venugopal, A.; Hinojos, D.; Magnuson, C.W.; McDonnell, S.; Colombo, L.; Vogel, E.M.; Ruoff, R.S.; Wallace, R.M. The effect of chemical residues on the physical and electrical properties of chemical vapor deposited graphene transferred to SiO₂. *Appl. Phys. Lett.* **2011**, *99*, 122108. [CrossRef]

49. Suk, J.W.; Kitt, A.; Magnuson, C.W.; Hao, Y.; Ahmed, S.; An, J.; Swan, A.K.; Goldberg, B.B.; Ruoff, R.S. Transfer of CVD-Grown Monolayer Graphene onto Arbitrary Substrates. *ACS Nano* **2011**, *5*, 6916–6924. [CrossRef] [PubMed]

50. Yu, Q.; Lian, J.; SiripongIt, S.; Li, H.; Chen, Y.P.; Pei, S.-S. Graphene segregated on Ni surfaces and transferred to insulators. *Appl. Phys. Lett.* **2008**, *93*, 113103. [CrossRef]

51. De Arco, L.G.; Zhang, Y.; Kumar, A.; Zhou, C. Synthesis, Transfer, and Devices of Single- and Few-Layer Graphene by Chemical Vapor Deposition. *IEEE Trans. Nanotechnol.* **2009**, *8*, 135–138. [CrossRef]

52. Varykhalov, A.; Rader, O. Graphene grown on Co(0001) films and islands: Electronic structure and its precise magnetization dependence. *Phys. Rev. B* **2009**, *80*. [CrossRef]

53. Sutter, P.W.; Flege, J.-I.; Sutter, E.A. Epitaxial graphene on ruthenium. *Nat. Mater.* **2008**, *7*, 406–411. [CrossRef] [PubMed]

54. Coraux, J.; N'Diaye, A.T.; Busse, C.; Michely, T. Structural Coherency of Graphene on Ir(111). *Nano Lett.* **2008**, *8*, 565–570. [CrossRef] [PubMed]

55. Sutter, P.; Sadowski, J.T.; Sutter, E. Graphene on Pt(111): Growth and substrate interaction. *Phys. Rev. B* **2009**, *80*. [CrossRef]

56. Miniussi, E.; Pozzo, M.; Baraldi, A.; Vesselli, E.; Zhan, R.R.; Comelli, G.; Mentes, T.O.; Niño, M.A.; Locatelli, A.; Lizzit, S.; et al. Thermal Stability of Corrugated Epitaxial Graphene Grown on Re(0001). *Phys. Rev. Lett.* **2011**, *106*. [CrossRef] [PubMed]

57. Kwon, S.Y.; Ciobanu, C.V.; Petrova, V.; Shenoy, V.B.; Bareno, J.; Gambin, V.; Petrov, I.; Kodambaka, S. Growth of Semiconducting Graphene on Palladium. *Nano Lett.* **2009**, *9*, 3985–3990. [CrossRef] [PubMed]

58. Zhang, Y.; Gomez, L.; Ishikawa, F.N.; Madaria, A.; Ryu, K.; Wang, C.; Badmaev, A.; Zhou, C. Comparison of Graphene Growth on Single-Crystalline and Polycrystalline Ni by Chemical Vapor Deposition. *J. Phys. Chem. Lett.* **2010**, *1*, 3101–3107. [CrossRef]

59. Massalski, T.B.; Okamoto, H.; Subramanian, P.R.; Kacprzak, L. *ASM Handbook: Alloy Phase Diagrams*; ASM International: Materials Park, OH, USA, 2002; p. 3.

60. Li, X.; Colombo, L.; Ruoff, R.S. Graphene Films: Synthesis of Graphene Films on Copper Foils by Chemical Vapor Deposition (Adv. Mater. 29/2016). *Adv. Mater.* **2016**, *28*, 6264. [CrossRef]

61. Chen, S.; Cai, W.; Piner, R.D.; Suk, J.W.; Wu, Y.; Ren, Y.; Kang, J.; Ruoff, R.S. Synthesis and Characterization of Large-Area Graphene and Graphite Films on Commercial Cu–Ni Alloy Foils. *Nano Lett.* **2011**, *11*, 3519–3525. [CrossRef]

62. Eizenberg, M.; Blakely, J.M. Carbon interaction with nickel surfaces: Monolayer formation and structural stability. *J. Chem. Phys.* **1979**, *71*, 3467–3477. [CrossRef]

63. Wu, Y.; Chou, H.; Ji, H.; Wu, Q.; Chen, S.; Jiang, W.; Hao, Y.; Kang, J.; Ren, Y.; Piner, R.D.; et al. Growth Mechanism and Controlled Synthesis of AB-Stacked Bilayer Graphene on Cu–Ni Alloy Foils. *ACS Nano* **2012**, *6*, 7731–7738. [CrossRef]

64. Shelton, J.; Patil, H.; Blakely, J. Equilibrium segregation of carbon to a nickel (111) surface: A surface phase transition. *Surf. Sci.* **1974**, *43*, 493–520. [CrossRef]

65. Li, X.; Cai, W.; Colombo, L.; Ruoff, R.S. Evolution of Graphene Growth on Ni and Cu by Carbon Isotope Labeling. *Nano Lett.* **2009**, *9*, 4268–4272. [CrossRef] [PubMed]

66. Chan, J.; Venugopal, A.; Pirkle, A.; McDonnell, S.; Hinojos, D.; Magnuson, C.W.; Ruoff, R.S.; Colombo, L.; Wallace, R.M.; Vogel, E.M. Reducing Extrinsic Performance-Limiting Factors in Graphene Grown by Chemical Vapor Deposition. *ACS Nano* **2012**, *6*, 3224–3229. [CrossRef] [PubMed]

67. Li, X.; Zhu, Y.; Cai, W.; Borysiak, M.; Han, B.; Chen, D.; Piner, R.D.; Colombo, L.; Ruoff, R.S. Transfer of Large-Area Graphene Films for High-Performance Transparent Conductive Electrodes. *Nano Lett.* **2009**, *9*, 4359–4363. [CrossRef] [PubMed]

68. Wang, G.; Zhang, M.; Liu, S.; Xie, X.; Ding, G.; Wang, Y.; Chu, P.K.; Gao, H.; Ren, W.; Yuan, Q.; et al. Synthesis of Layer-Tunable Graphene: A Combined Kinetic Implantation and Thermal Ejection Approach. *Adv. Funct. Mater.* **2015**, *25*, 3666–3675. [CrossRef]

69. Wan, N.; Lin, T.; Bi, H.; Huang, F.; Xie, X.; Chen, I.-W.; Jiang, M. Autonomously Controlled Homogenous Growth of Wafer-Sized High-Quality Graphene via a Smart Janus Substrate. *Adv. Funct. Mater.* **2012**, *22*, 1033–1039. [CrossRef]

70. Choi, J.S.; Choi, H.; Kim, K.-C.; Jeong, H.Y.; Yu, Y.-J.; Kim, J.T.; Shin, J.-W.; Cho, H.; Choi, C.-G. Facile fabrication of properties-controllable graphene sheet. *Sci. Rep.* **2016**, *6*, 24525. [CrossRef]

71. Kang, D.; Kim, W.-J.; Lim, J.A.; Song, Y.-W. Direct Growth and Patterning of Multilayer Graphene onto a Targeted Substrate without an External Carbon Source. *ACS Appl. Mater. Interfaces* **2012**, *4*, 3663–3666. [CrossRef]

72. Bai, J.; Huang, Y. Fabrication and electrical properties of graphene nanoribbons. *Mater. Sci. Eng. R Rep.* **2010**, *70*, 341–353. [CrossRef]

73. Kim, W.J.; Debnath, P.C.; Lee, J.; Lee, J.H.; Lim, D.S.; Song, Y.W. Transfer-free synthesis of multilayer graphene using a single-step process in an evaporator and formation confirmation by laser mode-locking. *Nanotechnology* **2013**, *24*, 365603. [CrossRef]

74. Kwak, J.; Chu, J.H.; Choi, J.-K.; Park, S.-D.; Go, H.; Kim, S.Y.; Park, K.; Kim, Y.-W.; Yoon, E.; Kodambaka, S.; et al. Near room-temperature synthesis of transfer-free graphene films. *Nat. Commun.* **2012**, *3*, 645. [CrossRef]

75. Isett, L.; Blakely, J. Segregation isosteres for carbon at the (100) surface of nickel. *Surf. Sci.* **1976**, *58*, 397–414. [CrossRef]

76. Vang, R.T.; Honkala, K.; Dahl, S.; Vestergaard, E.K.; Schnadt, J.; Lægsgaard, E.; Clausen, B.S.; Nørskov, J.K.; Besenbacher, F. Controlling the catalytic bond-breaking selectivity of Ni surfaces by step blocking. *Nat. Mater.* **2005**, *4*, 160–162. [CrossRef]

77. Tan, X.; Yang, G. Catalytic bond-breaking selectivity in the ethylene decomposition on Ni surfaces: Kinetic Monte Carlo sim-ulations. *J. Phys. Chem. C* **2008**, *112*, 4219–4225. [CrossRef]

78. Yang, G.; Kim, H.-Y.; Jang, S.; Kim, J. Transfer-Free Growth of Multilayer Graphene Using Self-Assembled Monolayers. *ACS Appl. Mater. Interfaces* **2016**, *8*, 27115–27121. [CrossRef]

79. Love, J.C.; Estroff, L.A.; Kriebel, J.K.; Nuzzo, R.G.; Whitesides, G.M. Self-Assembled Monolayers of Thiolates on Metals as a Form of Nanotechnology. *Chem. Rev.* **2005**, *105*, 1103–1170. [CrossRef]

80. Chaki, N.K.; Vijayamohanan, K. Self-assembled monolayers as a tunable platform for biosensor applications. *Biosens. Bioelectron.* **2002**, *17*, 1–12. [CrossRef]

81. Dabirian, A.; Byranvand, M.M.; Naqavi, A.; Kharat, A.N.; Taghavinia, N. Self-Assembled Monolayer of Wavelength-Scale Core–Shell Particles for Low-Loss Plasmonic and Broadband Light Trapping in Solar Cells. *ACS Appl. Mater. Interfaces* **2016**, *8*, 247–255. [CrossRef] [PubMed]

82. Debnath, P.C.; Park, J.; Scott, A.M.; Lee, J.; Lee, J.H.; Song, Y.-W. In Situ Synthesis of Graphene with Telecommunication Lasers for Nonlinear Optical Devices. *Adv. Opt. Mater.* **2015**, *3*, 1264–1272. [CrossRef]

83. Debnath, P.C.; Uddin, S.; Song, Y.-W. Ultrafast All-Optical Switching Incorporatingin SituGraphene Grown along an Optical Fiber by the Evanescent Field of a Laser. *ACS Photon* **2017**, *5*, 445–455. [CrossRef]

84. Xiong, W.; Zhou, Y.S.; Jiang, L.J.; Sarkar, A.; Mahjouri-Samani, M.; Xie, Z.Q.; Gao, Y.; Ianno, N.J.; Jiang, L.; Lu, Y.F. Single-Step Formation of Graphene on Dielectric Surfaces. *Adv. Mater.* **2013**, *25*, 630–634. [CrossRef]

85. Yan, Z.; Peng, Z.; Sun, Z.; Yao, J.; Zhu, Y.; Liu, Z.; Ajayan, P.M.; Tour, J.M. Growth of Bilayer Graphene on Insulating Substrates. *ACS Nano* **2011**, *5*, 8187–8192. [CrossRef] [PubMed]

86. Kim, J.; Lee, G.; Kim, J. Wafer-scale synthesis of multi-layer graphene by high-temperature carbon ion implantation. *Appl. Phys. Lett.* **2015**, *107*, 033104. [CrossRef]

87. Song, H.J.; Son, M.; Park, C.; Lim, H.; Levendorf, M.P.; Tsen, A.W.; Park, J.; Choi, H.C. Large scale metal-free synthesis of graphene on sapphire and transfer-free device fabrication. *Nanoscale* **2012**, *4*, 3050–3054. [CrossRef] [PubMed]

88. Jerng, S.K.; Yu, D.S.; Kim, Y.S.; Ryou, J.; Hong, S.; Kim, C.; Yoon, S.; Efetov, D.K.; Kim, P.; Chun, S.H. Nanocrystalline Graphite Growth on Sapphire by Carbon Molecular Beam Epitaxy. *J. Phys. Chem. C* **2011**, *115*, 4491–4494. [CrossRef]

89. Wei, D.; Mitchell, J.I.; Tansarawiput, C.; Nam, W.; Qi, M.; Ye, P.D.; Xu, X. Laser direct synthesis of graphene on quartz. *Carbon* **2013**, *53*, 374–379. [CrossRef]

90. Yang, W.; He, C.; Zhang, L.; Wang, Y.; Shi, Z.; Cheng, M.; Xie, G.; Wang, D.; Yang, R.; Shi, D.; et al. Growth, Characterization, and Properties of Nanographene. *Small* **2012**, *8*, 1429–1435. [CrossRef] [PubMed]

91. Rümmeli, M.H.; Bachmatiuk, A.; Scott, A.M.; Börrnert, F.; Warner, J.H.; Hoffmann, V.H.; Lin, J.-H.; Cuniberti, G.; Büchner, B. Direct Low-Temperature Nanographene CVD Synthesis over a Dielectric Insulator. *ACS Nano* **2010**, *4*, 4206–4210. [CrossRef]

92. Scott, A.; Dianat, A.; Börrnert, F.; Bachmatiuk, A.; Warner, J.H.; Borowiak-Paleń, E.; Knupfer, M.; Büchner, B.; Cuniberti, G.; Rümmeli, M.H. The catalytic potential of high-κ dielectrics for graphene formation. *Appl. Phys. Lett.* **2011**, *98*, 073110. [CrossRef]

93. Miranda, E.; O'Connor, E.; Hughes, G.; Casey, P.; Cherkaoui, K.; Monaghan, S.; Long, R.; O'Connell, D.; Hurley, P. Degradation dynamics and breakdown of MgO gate oxides. *Microelectron. Eng.* **2009**, *86*, 1715–1717. [CrossRef]

94. Seo, Y.; Lee, S.; An, I.; Song, C.; Jeong, H. Conduction mechanism of leakage current due to the traps in ZrO_2 thin film. *Semicond. Sci. Technol.* **2009**, *24*. [CrossRef]

95. Park, J.; Lee, J.; Choi, J.-H.; Hwang, D.K.; Song, Y.-W. Growth, Quantitative Growth Analysis and Applications of Graphene on γ-Al2O3 catalysts. *Sci. Rep.* **2015**, *5*, 11839. [CrossRef] [PubMed]

96. Park, J.; Kim, K.H.; Kim, J.; Lee, C.J.; Shim, J.H.; Song, Y.-W.; Ha, J.S. Catalyst-free growth of readily detachable nanographene on alumina. *J. Mater. Chem. C* **2013**, *1*, 6438–6445. [CrossRef]

97. Ago, H.; Ogawa, Y.; Tsuji, M.; Mizuno, S.; Hibino, H. Catalytic Growth of Graphene: Toward Large-Area Single-Crystalline Graphene. *J. Phys. Chem. Lett.* **2012**, *3*, 2228–2236. [CrossRef]

98. Han, G.H.; Güneş, F.; Bae, J.J.; Kim, E.S.; Chae, S.J.; Shin, H.-J.; Choi, J.-Y.; Pribat, D.; Lee, Y.H. Influence of Copper Morphology in Forming Nucleation Seeds for Graphene Growth. *Nano Lett.* **2011**, *11*, 4144–4148. [CrossRef] [PubMed]

99. He, C.; Shi, Z.; Zhang, L.; Yang, W.; Yang, R.; Shi, D.; Zhang, G. Multilevel Resistive Switching in Planar Graphene/SiO_2 Nanogap Structures. *ACS Nano* **2012**, *6*, 4214–4221. [CrossRef]

100. Zhang, L.; Shi, Z.; Wang, Y.; Yang, R.; Shi, D.; Zhang, G. Catalyst-free growth of nanographene films on various substrates. *Nano Res.* **2011**, *4*, 315–321. [CrossRef]

101. Lee, M.; Park, K.; Park, J.; Choi, D.K.; Song, Y.W. Oxygen-Dependent Synthesis of Graphene on γ-Alumina Catalyst. *Adv. Mater. Interfaces* **2017**, *4*, 1700603. [CrossRef]

102. Gan, L.; Luo, Z. Turning off Hydrogen to Realize Seeded Growth of Subcentimeter Single-Crystal Graphene Grains on Copper. *ACS Nano* **2013**, *7*, 9480–9488. [CrossRef]

103. Karnatak, P.; Sai, T.P.; Goswami, S.; Ghatak, S.; Kaushal, S.; Ghosh, A. Current crowding mediated large contact noise in graphene field-effect transistors. *Nat. Commun.* **2016**, *7*, 13703. [CrossRef] [PubMed]

104. Velez-Fort, E.; Ouerghi, A.; Silly, M.; Eddrief, M.; Shukla, A.; Sirtti, F.; Marangolo, M. Atomic oxidation of large area epitaxial graphene on 4H-SiC (0001). *Appl. Phys. Lett.* **2014**, *104*, 093109. [CrossRef]

105. Xia, F.; Farmer, D.B.; Lin, Y.-M.; Avouris, P. Graphene Field-Effect Transistors with High On/Off Current Ratio and Large Transport Band Gap at Room Temperature. *Nano Lett.* **2010**, *10*, 715–718. [CrossRef] [PubMed]

106. Wischert, R.; Laurent, P.; Copéret, C.; Delbecq, F.O.; Sautet, P. γ-Alumina: The essential and unexpected role of water for the structure, stability, and reactivity of "defect" sites. *J. Am. Chem. Soc.* **2012**, *134*, 14430–14449. [CrossRef]

107. Wischert, R.; Copéret, C.; Delbecq, F.; Sautet, P. Optimal Water Coverage on Alumina: A Key to Generate Lewis Acid-Base Pairs that are Reactive Towards the C—H Bond Activation of Methane. *Angew. Chem.* **2011**, *123*, 3260–3263. [CrossRef]

108. Yang, J.; Tang, L.L.; Luo, W.; Shen, J.; Zhou, D.H.; Feng, S.L.; Wei, X.Z.; Shi, H.F. Light Trapping in Conformal Graphene/Silicon Nanoholes for High-Performance Photodetectors. *ACS Appl. Mater. Inter.* **2019**, *11*, 30421–30429. [CrossRef]

109. Uddin, S.; Song, Y.W. Atomic Carbon Spraying: Direct Growth of Graphene on Customized 3D Surfaces of Ultrafast Optical Devices. *Adv. Opt. Mater.* **2020**, *8*, 1902091. [CrossRef]

110. Bonaccorso, F.; Sun, Z.; Hasan, T.; Ferrari, A.C. Graphene photonics and optoelectronics. *Nat. Photon* **2010**, *4*, 611–622. [CrossRef]
111. Sun, Z.; Hasan, T.; Torrisi, F.; Popa, D.; Privitera, G.; Wang, F.; Bonaccorso, F.; Basko, D.M.; Ferrari, A.C. Graphene Mode-Locked Ultrafast Laser. *ACS Nano* **2010**, *4*, 803–810. [CrossRef] [PubMed]
112. Bao, Q.; Zhang, H.; Wang, Y.; Ni, Z.; Yan, Y.; Shen, Z.X.; Loh, K.P.; Tang, D.Y. Atomic-Layer Graphene as a Saturable Absorber for Ultrafast Pulsed Lasers. *Adv. Funct. Mater.* **2009**, *19*, 3077–3083. [CrossRef]
113. Song, Y.-W.; Jang, S.-Y.; Han, W.-S.; Bae, M.-K. Graphene mode-lockers for fiber lasers functioned with evanescent field interaction. *Appl. Phys. Lett.* **2010**, *96*, 051122. [CrossRef]
114. Chang, Y.M.; Kim, H.; Lee, J.H.; Song, Y.-W. Multilayered graphene efficiently formed by mechanical exfoliation for nonlinear saturable absorbers in fiber mode-locked lasers. *Appl. Phys. Lett.* **2010**, *97*, 211102. [CrossRef]
115. Popa, D.; Sun, Z.; Hasan, T.; Torrisi, F.; Wang, F.; Ferrari, A.C. Graphene Q-switched, tunable fiber laser. *Appl. Phys. Lett.* **2011**, *98*, 073106. [CrossRef]
116. Zhang, H.; Tang, D.; Knize, R.J.; Zhao, L.; Bao, Q.; Loh, K.P. Graphene mode locked, wavelength-tunable, dissipative soliton fiber laser. *Appl. Phys. Lett.* **2010**, *96*, 111112. [CrossRef]
117. Zhang, H.; Tang, D.Y.; Zhao, L.M.; Bao, Q.L.; Loh, K.P. Large energy mode locking of an erbium-doped fiber laser with atomic layer graphene. *Opt. Express* **2009**, *17*, 17630–17635. [CrossRef] [PubMed]
118. Zhang, H.; Tang, D.; Zhao, L.; Bao, Q.; Loh, K.P. Vector dissipative solitons in graphene mode locked fiber lasers. *Opt. Commun.* **2010**, *283*, 3334–3338. [CrossRef]
119. Martinez, A.; Fuse, K.; Yamashita, S. Mechanical exfoliation of graphene for the passive mode-locking of fiber lasers. *Appl. Phys. Lett.* **2011**, *99*, 121107. [CrossRef]
120. Zhao, L.M.; Tang, D.Y.; Zhang, H.; Wu, X.; Bao, Q.; Loh, K.P. Dissipative soliton operation of an ytterbium-doped fiber laser mode locked with atomic multilayer graphene. *Opt. Lett.* **2010**, *35*, 3622–3624. [CrossRef]
121. Bao, Q.; Zhang, H.; Ni, Z.; Wang, Y.; Polavarapu, L.; Shen, Z.; Xu, Q.-H.; Tang, D.; Loh, K.P. Monolayer graphene as a saturable absorber in a mode-locked laser. *Nano Res.* **2011**, *4*, 297–307. [CrossRef]
122. Chow, K.K.; Yamashita, S. Four-wave mixing in a single-walled carbon-nanotube-deposited D-shaped fiber and its application in tunable wavelength conversion. *Opt. Express* **2009**, *17*, 15608–15613. [CrossRef] [PubMed]
123. Uddin, S.; Debnath, P.C.; Park, K.; Song, Y.-W. Nonlinear Black Phosphorus for Ultrafast Optical Switching. *Sci. Rep.* **2017**, *7*, srep43371. [CrossRef] [PubMed]